ELSEVIER

Journal of University of Science and Technology Beijing
Volume 15, Number 6, December 2008, Page 816

Materials

Pseudo-capacitance of ruthenium oxide/carbon black composites for electrochemical capacitors

Xiaofeng Wang[1)], *Dianbo Ruan*[1)], *Peng Wang*[2)], *and Yiqiang Lu*[2)]

1) Department of Precision Instruments and Mechanics, Tsinghua University, Beijing 100084, China
2) School of Applied Science, University of Science and Technology BeiJing, Beijing 100083, China
(Received 2007-12-13)

Abstract: Hydrous ruthenium oxide was formed by a new process. The precursor was obtained by mixing the aqueous solutions of $RuCl_3 \cdot xH_2O$ and $NaHCO_3$. The addition of $NaHCO_3$ led to the formation of an oxide with extremely fine RuO_2 particles forming a porous network structure in the oxide electrode. Polyethylene glycol was added as a controller to partly inhibit the sol-gel reaction. The rate capacitance of 530 $F \cdot g^{-1}$ was measured for the powder formed at an optimal annealing temperature of 210°C. Several details concerning this new material, including crystal structure, particle size as a function of temperature, and electrochemical properties, were also reported. In addition, the rate capacitance of the composite electrode reached 800 $F \cdot g^{-1}$ after carbon black was added. By using the modified electrode of a RuO_2/carbon black composite electrode, the electrochemical capacitor exhibits high energy density and stable power characteristics. The values of specific energy and maximum specific power of 24 $Wh \cdot kg^{-1}$ and 4 $kW \cdot kg^{-1}$, respectively, are demonstrated for a cell voltage between 0 and 1 V.

Key words: electrochemical capacitor; ruthenium oxide; polyethylene glycol; carbon black

1. Introduction

Super capacitors or electrochemical capacitors (ECs) have been recognized as a unique device exhibiting high-power characteristics with an acceptable capacity and long cycle life for energy storage/delivery and management in future power systems. The novel performance of this device usually results from the high specific surface area, as well as the highly reversible redox reactions of the electrode materials. Hence, porous activated carbon (PAC) [1-4], hydrous transition metal oxides [5-18], and conducting polymers [19-20] are the main components in the electrode materials of electrochemical capacitors.

RuO_2 is a promising electrode material that exhibits large electrochemical capacitance essential to supercapacitor application [5-11]. A RuO_2 electrode with a specific capacitance as high as 760 $F \cdot g^{-1}$ has been reported [5-6]. However, RuO_2 have a low porosity structure and the electrode material crystallizes as early as 175°C when the tendency of the rising rate capacitance stops. Thus, the reported 760 $F \cdot g^{-1}$ is only 80% of the theoretical value of 900 $F \cdot g^{-1}$. Due to the cost of ruthenium, there have been several studies of combining ruthenium oxide with other materials to form composite electrodes with the intention to increase the dispersion of ruthenium oxide in porous carbon matrix and/or surface [9-11]. PAC-RuO_x composites have been shown to be one of the most promising electrode materials for supercapacitors [5-10]. However, the result of Wang *et al.* [10] indicated that large particle size made from the sol-gel process blocked mesopores in the activated carbon, which lowered the double layer capacitance coming from carbon. In order to refine the particle size and increase the porosity of the powder, Wang prepared the ruthenium oxide/carbon composite through a colloidal method [11]. A certain amount of carbon was used to control the RuO_2 particle size. Both the particle size and the amount of carbon loaded were thought to be the factors of influencing the rate capacitance. The carbon loaded in the electrode was effective in raising the composite capacitance.

The purpose of this paper was to show the effects of

Corresponding author: Xiaofeng Wang, **E-mail:** xfw@tsinghua.edu.cn
Also available online at www.sciencedirect.com

annealing temperature on the capacitive performance of $RuO_2{\cdot}xH_2O$. The effect of polyethylene glycol controller on the surface characteristics of $RuO_2{\cdot}xH_2O$ was also investigated. Moreover, this investigation examined the dependence of supercapacitor performance on the content of carbon black. Supercapacitor performance was assessed *via* cyclic voltammetry (CV), charge-discharge studies (DC), and impedance analysis (AC). The nanostructure of $RuO_2{\cdot}xH_2O$ was examined by scanning electron micrograph (SEM) and thermogravimetric analyzer (TGA). A rating of power density and energy density of the devices was reported.

2. Experimental

The $RuO_2{\cdot}xH_2O$ powder was prepared by a new process described as follows. The required amount of $RuCl_3{\cdot}xH_2O$ was dissolved in a solvent of 50vol% ethanol to give a desired concentration (0.1 $mol{\cdot}L^{-1}$). For the preparation of the RuO_2/carbon composite electrode, the designed amount of carbon black was dispersed in the dilute $RuCl_3$ solution in advance. Then, the $NaHCO_3$ solution with a concentration of 0.3 $mol{\cdot}L^{-1}$ was added slowly into the $RuCl_3$ solution until the pH value reached to 5. During mixing, the $RuCl_3$ solution was stirred by a magnetic stirring bar. Following the adjustment of pH, the stirring was stopped, and black powders precipitated in clear NaCl solution. Polyethylene glycol was added to the solution as a controller, which partly inhibited the reaction and the reunion of particles. The particle size and configuration of the product could be controlled with polyethylene glycol [10]. The resulting product was separated from the solution by filtration. Polyethylene glycol dissolved in water could be separated in this way. Different composites with 10% and 20% carbon black loaded were synthesized with this technique. The powders were heated in air at 80°C for 10 h and then heated at various temperatures.

Polarizable capacitor electrodes could be manufactured according to the invention by conventional method known in Ref. [11]. Thus, the electro-active materials and water were mixed in a blender or kneader. The paste-like mixture obtained was then rolled to form flexible films with a thickness of 0.2 mm. This film-like raw material for electrodes was cut into disks. The disk electrodes were then mounted on a graphite collector. Two test cells were introduced in this paper. A beaker-type electrochemical cell equipped with a working electrode, a platinum counter electrode, and a saturated calomel electrode (SCE) reference electrode was used. The electrodes are simply dipped into the 38% H_2SO_4. These electrode were connected to a CHI660B system (Shanghai Chenhua Corporation), which drove the voltage in either direction sequentially at predetermined constant sweep rates. The sweep rate of 20 $mV{\cdot}s^{-1}$ was used during testing. Another cell was much more characteristic of an actual working device. The electrodes were pressed together and separated by a porous glass fiber separator. The voltages of the cell were measured during constant current charge/discharge.

The specific capacitance of the single electrode can be calculated from CV curves from

$$C_s = i / s \tag{1}$$

where i and s are the current response and the potential sweep rate (dV/dt), respectively. The average specific capacitance of the single electrode (C_s) in the potential range of 0-1 V *vs*. SCE is calculated by integrating oxidation currents in the CV curves.

The specific capacitance of the asymmetric capacitor can be evaluated from the charge/discharge test together with the following equation:

$$C = \frac{I\Delta t}{\Delta V} \tag{2}$$

where C is the capacitance (F), I is the discharge current (A), Δt is the time period for the potential change (s), ΔV is the potential change (V).

The real power density P_{real} ($W{\cdot}g^{-1}$) is determined from the constant current charge/discharge cycles as follows:

$$P_{real} = \frac{\Delta E \cdot I}{m} \tag{3}$$

where $\Delta E = (E_{max}+E_{min})/2$ with E_{max} as the potential at the begin of discharge (after the ohmic drop) and E_{min} at the end of discharge, and m the weight of active material in the electrodes (g).

Alternatively, the maximum specific power, P_{max} ($W{\cdot}g^{-1}$), is calculated as

$$P_{max} = \frac{U_0^2}{4Rm} \tag{4}$$

where U_0 is the potential at the end of charging (1 V) and R the equivalent serials resistance (ESR in Ω).

The real specific energy E_{real} ($J{\cdot}g^{-1}$) is defined as

$$E_{real} = \frac{CU_{max}^2}{2m} \tag{5}$$

where C is the system capacitance (F) for a cell, and U_{max} is the potential at the beginning of discharge.

3. Results and discussion

3.1. Electrochemical properties of RuO_2 annealed at different temperatures

The capacitance of ruthenium oxide materials was dependent on the sample annealing temperature. Fig. 1 shows the cyclic voltammograms of pure ruthenium oxide treated at different temperatures at a scan rate of 20 $mV \cdot s^{-1}$. The magnitude of the currents observed changes with annealing temperature. The anodic and cathodic currents increase with the increase of treatment temperature when T_s<210°C. The capacitance of the material is determined by integrating the anodic and cathodic charges according to Eq. (1). The materials heated at 210°C exhibit the highest voltammetric capacitance of 530 $F \cdot g^{-1}$. Moreover, the voltammograms of the electrode treated at different temperatures show increasing amounts of reversibility. It is found that heating the sample beyond 250°C decreases its capacitance to less than 230 $F \cdot g^{-1}$.

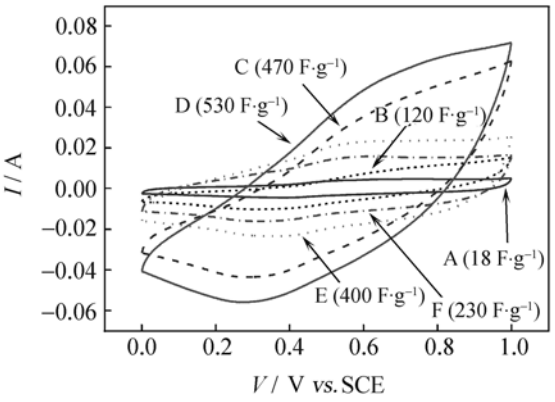

Fig. 1. CVs of the materials treated at different temperatures (line A: 100°C; line B: 150°C; line C: 200°C; line D: 210°C; line E: 230°C; line F: 250°C).

3.2. Thermal dynamic properties and SEM experiments

A computer-controlled thermogravimetric analyzer (TGA) and a differential scanning calorimeter (DSC) were used to study the weight change and enthalpic change during the thermal processes. The weight of powder decreased continuously as the temperature was increased from room temperature to 300°C. The line in Fig. 2 shows the derivative of the weight change as a function of temperature studied by TGA measurement at temperature scan rate of 2 $°C \cdot min^{-1}$. From the derivative of the change in weight, three peaks are obtained at temperatures of ~90°C and ~220°C and >250°C, at which $Ru(HCO_3)_3$, $RuO_2 \cdot xH_2O$, and RuO_2 are formed, respectively. Peak A at ~90°C is due to the vaporization of H_2O absorbed in the powder, and peak C after 250°C is due to the transition of $RuO_2 \cdot xH_2O$ to RuO_2, these are in agreement with result of Zheng and Jow [5-6]; hence, the final powder after crystallization is also RuO_2. Peak B at 210°C is related to the decomposition course of $Ru(HCO_3)_3$ releasing H_2O and CO_2 at the same time.

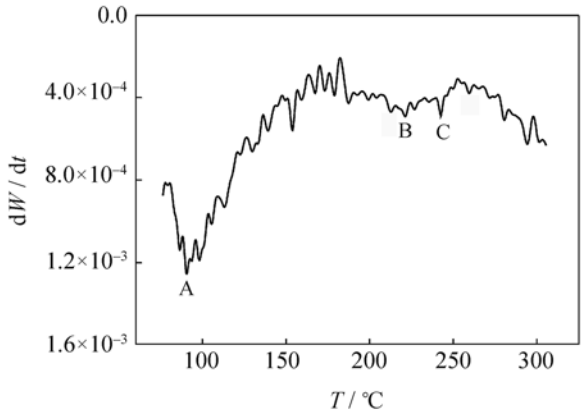

Fig. 2. Derivative weight loss as a function of annealing temperature.

Fig. 3 shows the SEM images of the electrode materials annealed at 100°C, 150°C, 210°C, and 250°C, respectively. Although the particles of the amorphous material heated at 100°C are ultrafine as shown in Fig. 3(a), the surface area of the electrode is very small for the ultrafine $Ru(HCO_3)_3$ particles to impinge and reunite together. Hence, the capacitance of the material heated at 100°C is only 18 $F \cdot g^{-1}$. When the material is heated at a higher temperature, the size of particles expanded and the active surface area of the material increased. A large amount of grains can be observed at 210°C as shown in Fig. 3(c). The inert $Ru(HCO_3)_3$ decomposed greatly and large amount of electro-active $RuO_2 \cdot xH_2O$ is produced at this temperature. The electrode exhibits tiny particle size (about 50 nm) and typical porosity, which will contribute to the high capacitance and low impedance. The maximum capacitance of 530 $F \cdot g^{-1}$ is achieved at T=210°C. With increasing annealing temperature, more $RuO_2 \cdot xH_2O$ material turns to be RuO_2 crystalline, and the crystalline size increases as shown in Fig. 3(d). This fact can explain the sharp decrease of capacitance at 230°C and above.

3.3. Cyclic voltammetry and impedance spectra of $RuO_2 \cdot xH_2O$/carbon black composites

Cyclic voltammetric measurement was helpful to understand the macroscopic electrochemical surface reaction at the electrode of the supercapacitor during the charging hand discharging process. Cyclic voltammetries on the $RuO_2 \cdot xH_2O$/carbon black nanocomposite electrodes were carried out to investigate the possible dominant mode of electrochemical energy

storage on the electrodes with different carbon loadings.

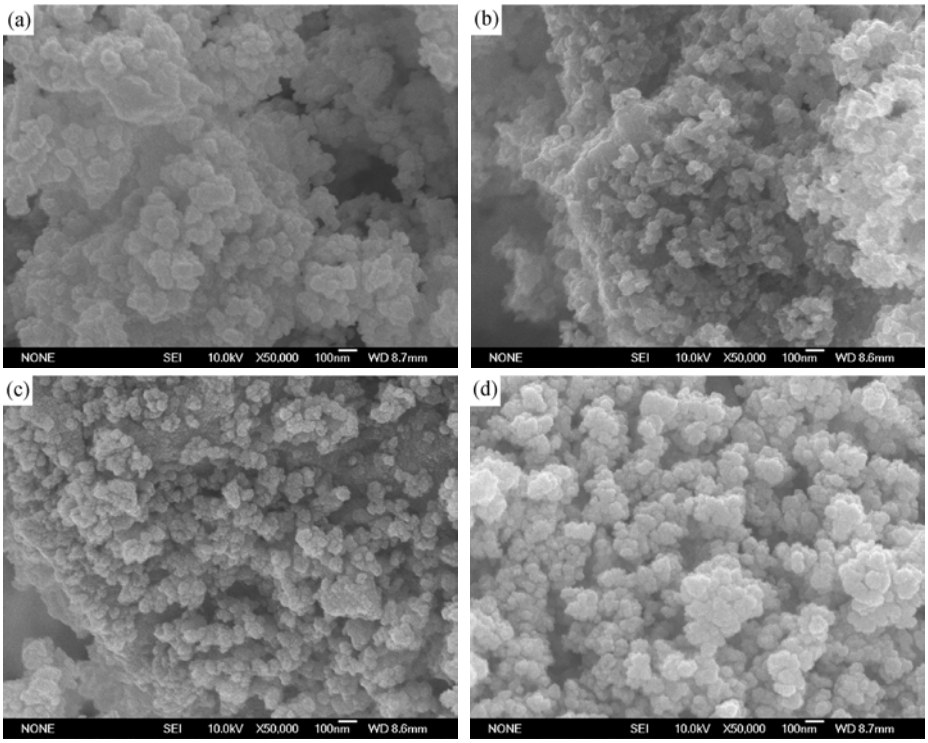

Fig. 3. SEM pictures of the electrode material annealed at different temperatures: (a) 100°C; (b) 150°C; (c) 210°C; (d) 250°C.

Fig. 4 shows the CV curves of the composite electrode in H_2SO_4 electrolyte at a scan rate of 20 $mV \cdot s^{-1}$. The charging and discharging cyclic voltammogram CV is close to a rectangular shape. Line A in Fig. 4 presents the cyclic voltammetric behaviors of pure $RuO_2 \cdot xH_2O$, and the pure ruthenium oxide electrode clearly shows faradaic redox reactions, which are observed at 0.6 and 0.4 V with respect to the SCE reference electrode representing the oxidation and reduction processes. The composite electrode showed a shape similar to the pure ruthenium oxide electrode basically, having the faradaic redox behavior. However, the electrochemical capacitance scale of the composite was much larger than that of the individual materials. We could say from the CV curves that the composite electrode showed the characteristics of a pseudo-capacitive electrode. This larger electrochemical capacitance arose from the uniform mixture of ruthenium oxide with carbon black, which increased effectively the active sites on oxide particles. The effective surface area of ruthenium oxide surrounded by carbon black was enhanced distinctly in the nanocomposite in comparison with the pure hydrous ruthenium oxide electrode, as mentioned previously. Further, porous carbon black also served as an electrolyte reservoir to reduce the ionic diffusion resistance regardless of charging/discharging the current density. The current responds of the electrode with 10% (line B) and 20% (line C) are enlarged greatly compared with the pure $RuO_2 \cdot xH_2O$ electrode. Fig. 4 shows that the rate capacitance increased sharply to 800 $F \cdot g^{-1}$ after 10% carbon black loaded, whereas the rate capacitance remains to be about 710 $F \cdot g^{-1}$ with 20% carbon black loaded. The 10% load is proved to be the optimal ratio for the composite obtained in this paper.

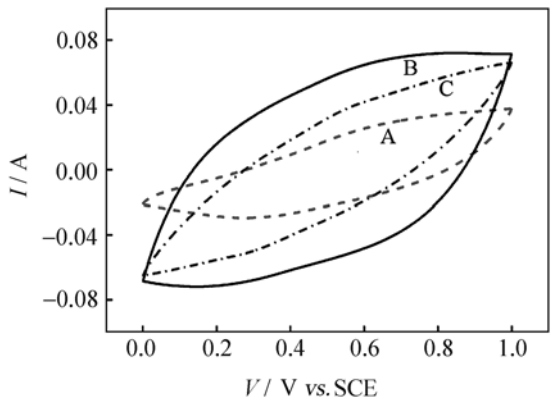

Fig. 4. CV curves of the RuO_2/carbon composites (line A: 0% carbon black load; line B: 10% carbon black load; line C: 20% carbon black load).

Fig. 5 presents the complex-plane plots for pure ruthenium oxide and the oxide/carbon black composite. Herein, we observe the complex-plane impedance of ruthenium oxide and composite to investigate the effect of carbon black on the internal resistance. The internal pseudo-transfer resistance of pure ruthenium oxide is very large, which will result in the serious

deterioration of capacitance at high discharge current. Although the internal resistance of the ruthenium oxide/carbon composite electrode is still large compared with the carbon black electrode, the internal resistance of the nanocomposite electrode is much smaller than that of pure ruthenium oxide. It is further proved the formation of the charge-transfer complex between the uniform dispersion carbon black and the ruthenium oxide matrix of the composite. The carbon black complex reduces the ion intercalation distance to a matter of nanometer, facilitates the charge-transfer and makes such resistance lower.

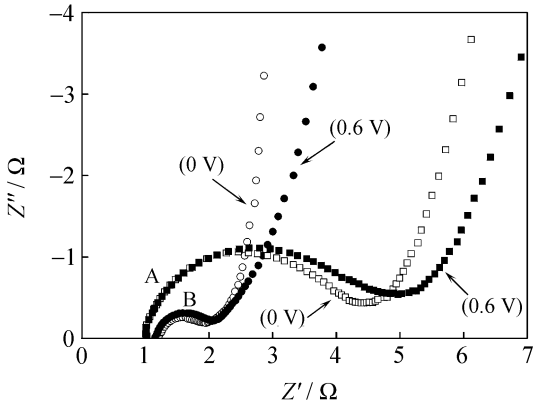

Fig. 5. Impedance spectra of the ruthenium oxide/carbon black composite (line A: pure $RuO_2{\cdot}xH_2O$ with 0% carbon black; line B: composite with 10% carbon black loaded).

3.4. Energy and power density

Fig. 6 shows the charge/discharge characteristics of a test capacitor composed of two oxide electrodes with 10% carbon black loaded. A small voltage drop at the beginning for high current density cases was due to the internal resistance of the capacitor. From Fig. 6, the energy deliverable efficiency can be easily estimated from the capacity ratio between the discharge and charge processes and is over 98%. The capacitance as a function of current density was measured. The results are shown in Fig. 7 for three capacitors made with different electrodes. It can be observed that the capacitance reduced at high current density. The relationship between capacitance and current density is strongly dependent on the carbon black loading of the electrode. For a capacitor that is made with the low porosity electrode of pure $RuO_2{\cdot}xH_2O$, the capacitance at a current of 25 mA is about 55% of that at low current (5 mA). The deliverable energy or energy density of the capacitor will also drop by the same ratio since the energy stored is proportional to the capacitance as shown in Eq. (5). For a capacitor that was composed of a electrode with 20% carbon black loaded, the power performance was improved significantly. It can be observed from Fig. 7 that the reduction of capacitance is less than 10% at a current density of 25 mA. By introducing the high porous carbon black into the electrode, both the power density and energy density of the capacitor were enhanced significantly.

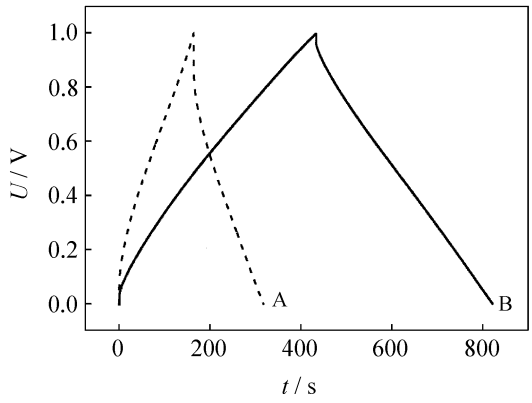

Fig. 6. Charge/discharge curve for a capacitor at a constant current of 5 mA (line A: 0% carbon black load; line B: 10% carbon black load).

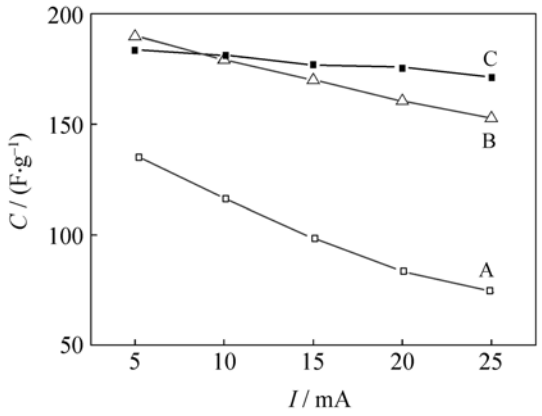

Fig. 7. Comparison of the capacitance decays of capacitors made with different electrodes as a function of discharge current (line A: 0% carbon black; line B: 10%; line C: 20%).

The Ragone plots of the capacitor summarize the performance of the three types of cells tested at various discharge currents (Fig. 8). The energy density and power density of the capacitor were calculated to be based on the active material only (the mass of bond, separator, current collector, and electrolyte was not included). The real energy density E_{real} of capacitor A increases from 4.5 $Wh{\cdot}kg^{-1}$ to 16.3 $Wh{\cdot}kg^{-1}$ when the real power density P_{real} decreases from 400 $W{\cdot}kg^{-1}$ to 110 $W{\cdot}kg^{-1}$. The maximum specific power density P_{max} of the cell reaches the value of 2.3 $kW{\cdot}kg^{-1}$ according to the Eq. (3). Obviously, the energy density and power density of capacitor A are poor. The E_{real} of capacitor C increases from 18 $Wh{\cdot}kg^{-1}$ to 24 $Wh{\cdot}kg^{-1}$ when P_{real} decreases from 500 $W{\cdot}kg^{-1}$ to 110 $W{\cdot}kg^{-1}$, which means that capacitor C is capable of delivering high power without profound loss in energy. The maximum specific power density of capacitor C

reaches the value of 4 $kW \cdot kg^{-1}$.

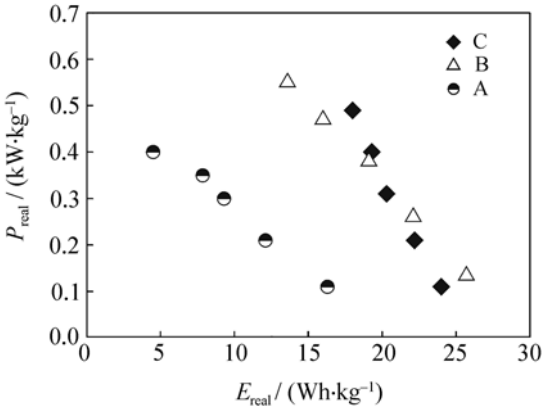

Fig. 8. Ragone plot of a combined capacitor (working voltage 1.0 V, current ranged from 5 mA/cm^2 to 25 mA/cm^2).

4. Conclusions

Ruthenium oxide with a smaller particle size and a higher porosity was prepared by a process using $RuCl_3 \cdot xH_2O$ and $NaHCO_3$ solution. Several details concerning this new material, including crystal structure, particle size as a function of temperature, and electrochemical properties, were also reported. The performance of supercapacitors made with $RuO_2 \cdot xH_2O$ and $RuO_2 \cdot xH_2O$/carbon black composite electrodes were demonstrated. The results show that by introducing high porous carbon black into the electrode, both the power density and energy density of the capacitor are enhanced significantly. The specific capacitance of over 800 $F \cdot g^{-1}$ is obtained in the composite electrode with 10% carbon black loaded. With these properties, the $RuO_2 \cdot xH_2O$/carbon black composite is an excellent material for EC capacitors.

References

[1] B.E. Conway, Transition from "supercapacitor" to "battery" behavior in electrochemical energy storage, *J. Electrochem. Soc.*, 138(1991), No.6, p.1539.

[2] R.A. Huggins, Supercapacitors and electrochemical pulse sources, *Solid State Ionics*, 134(2000), No.1-2, p.179.

[3] C. Vix-Guterl, S. Saadallah, and K. Jurewicz, Supercapacitor electrodes from new ordered porous carbon materials obtained by a templating procedure, *Mater. Sci. Eng. B*, 108(2004), No.1, p.148.

[4] X.F. Wang, D.B. Ruan, and Z. You, Performance of a 60 F carbon nanotubes-based supercapacitor for hybrid power sources, *J. Univ. Sci. Technol. Beijing*, 12(2005), No.3, p.267.

[5] J.P. Zheng and T.R. Jow, A new charge storage mechanism for electrochemical capacitors, *J. Electrochem. Soc.*, 142(1995), No.1, p.6.

[6] J.P. Zheng and T.R. Jow, High energy and high power density electrochemical capacitors, *J. Power Sources*, 62(1996), No.2, p.155.

[7] N.L. Wu, S.L. Kuo, and M.H. Lee, Preparation and optimization of RuO_2-impregnated SnO_2 xerogel supercapacitor, *J. Power Sources*, 104(2002), No.1, p.62.

[8] P.M. Wilde, T.J. Guther, and R. Oesten, Strontium ruthenate perovskite as the active material for supercapacitors, *J. Electroanal. Chem.*, 461(1999), No.1-2, p.154.

[9] C.C. Hu and C.C. Wang, Improving the utilization of ruthenium oxide within thick carbon-ruthenium oxide composites by annealing and anodizing for electrochemical supercapacitors, *Electrochem. Commun.*, 4(2002), No.7, p.554.

[10] X.F. Wang, D.Z. Wang, and J. Liang, Carbon nanotube capacitor materials loaded with different amounts of ruthenium oxide, *Acta Phys. Chim. Sin.*, 19(2003), No.6, p.509.

[11] X.F. Wang, D.B. Ruan, and Z. You, Ruthenium oxide with high rate pseudocapacitance prepared by a new sol-gel process, *Chin. J. Chem. Phys.*, 19(2006), No.4, p.341.

[12] C.Z. Deng and K.C. Cai, Improved porous mixture of molybdenum nitride and tantalum oxide as a charge storage materials, *J. Electrochem. Soc.*, 145(1998), No.4, p.61.

[13] J.H. Jiang and A. Kucernak, Electrochemical supercapacitor material based on manganese oxide: preparation and characterization, *Electrochim Acta*, 47(2002), No.15, p.2381.

[14] K.W. Nam, W.S. Yoon, and K.B. Kim, X-ray absorption spectroscopy studies of nickel oxide thin film electrodes for supercapacitors, *Electrochim. Acta*, 47(2002), No.19, p.3201.

[15] K.C. Liu and M.A. Anderson, Porous nickel oxide/nickel films for electrochemical capacitors, *J. Electrochem. Soc.*, 143(1996), No.1, p.124.

[16] V. Srinivasan and J.W. Weidner, An electrochemical route for making porous nickel oxide electrochemical capacitors, *J. Electrochem. Soc.*, 144(1997), No.8, p.210.

[17] C. Lin, A.J. Ritter, and B.N. Popov, Characterization of sol-gel derived cobalt oxide xergels as electrochemical capacitor, *J. Electrochem. Soc.*, 145(1998), No.12, p.4097.

[18] X.F. Wang and Y.Q. Cao, Performance of a combined capacitor based on ultrafine nickel oxide/carbon nanotubes composite electrodes, *J. Univ. Sci. Technol. Beijing*, 11(2004), No.6, p.533.

[19] P. Sivaraman, V.R. Hande, V.S. Mishra, *et al.*, All-solid supercapacitor based on polyaniline and sulfonated poly (ether ether ketone), *J. Power Sources*, 124(2003), No.1, p.351.

[20] A.M. White and R.C.T. Slade, Polymer electrodes doped with heteropolymetallates and their use within solid-state supercapacitor, *Synthetic metals*, 139 (2003), No.1, p.123.